Nanotechnology **20** (2009) 315301 (7pp) doi:10.1088/0957-4484/20/31/315301

Brilliant molecular nanocrystals emerging from sol–gel thin films: towards a new generation of fluorescent biochips

E Dubuisson[1,2], V Monnier[1], N Sanz-Menez[1], B Boury[3], Y Usson[4], R B Pansu[5] and A Ibanez[1]

[1] Institut Néel, CNRS & Université Joseph Fourier, UPR 2940, BP166, F-38042 Grenoble Cedex 9, France
[2] Genewave, XTEC, Bâtiment 404, Ecole Polytechnique, F-91128 Palaiseau Cedex, France
[3] Université Montpellier 2, Département de Chimie, Institut Charles Gerhardt, UMR 5253 CNRS, cc 1701, Place E Bataillon, F-34095 Montpellier Cedex 5, France
[4] TIMC-IMAG, UMR 5525 CNRS, Université Joseph Fourier, Domaine de la Merci, F-38706 La Tronche Cedex, France
[5] Laboratoire de Photophysique et de Photochimie Supramoléculaire et Macromoléculaire, CNRS, UMR 8531, ENS Cachan, F-94235 Cachan Cedex, France

E-mail: alain.ibanez@grenoble.cnrs.fr

Received 24 April 2009, in final form 8 June 2009
Published 13 July 2009
Online at stacks.iop.org/Nano/20/315301

Abstract
To develop highly sensitive biosensors, we made directly available to biological aqueous solutions organic nanocrystals previously grown in the pores of sol–gel films. Through the controlled dissolution of the sol–gel surface, we obtained emerging nanocrystals that remained strongly anchored to the sol–gel coating for good mechanical stability of the final sensing device. We demonstrated that in the presence of a solution of DNA functionalized with a molecular probe, the nanocrystal fluorescence is strongly quenched by Förster resonance energy transfer thus opening the way towards very sensitive fluorescent biosensors through biomolecules grafted onto fluorescent nanocrystals. Finally, this controlled dissolution, involving weak concentrated NaOH solution, is a generic process that can be used for the thinning of any kind of sol–gel layer.

(Some figures in this article are in colour only in the electronic version)

1. Introduction

In the last few years, DNA and protein biochips have become a powerful tool in clinical research, in particular for the development of diagnostic tests and new therapies. To detect the interaction between a probe and a targeted biomolecule on a chip microarray [1] numerous kinds of labels can be used: radioisotopes [2], chemiluminescent enzymes [3], metallic nanoparticles [4], fluorescent quantum dots (QDs) [5], or dyes [6]. The most sensitive method of labeling is radioactivity, but the use of ^{32}P or ^{125}I radioelements presents serious drawbacks [7] such as risks of contamination, delicate experimental set-up, and the problem of waste disposal. The other methods involve several chemical amplification steps by PCR (polymerase chain reaction) to obtain a sufficient amount of DNA molecules to be detected but they are long, expensive, and are not adapted to the detection of precious and rare clinical samples or the detection of weakly expressed genes and proteins [8]. Thus, even if microarrays have a large screening potential of a high number of samples for multiple and simultaneous analyses, they are under-exploited due to a lack of sensitivity. Indeed, although the theoretical detection limit was predicted to be a few femtograms or less [9], it has been difficult in practice to generate detectable signals for picograms of analyte in solution [10]. Moreover, in complex solutions containing several analytes, the relative sensitivity is expected to be even lower. In this context, there is a real need for more sensitive labels to improve current biochip microarrays, particularly for protein biochips, where

the noise level is usually higher than that of DNA biochips because of non-specific adsorptions [11]. Fluorescence methods present several unique experimental features such as large ranges of excitation and emission wavelengths, high quantum yields, and convenient fluorescence lifetimes: not too short for efficient temporal discrimination of short-lived fluorescence interference from scattered excitation light [12]. This allows detecting by typical fluorimeters quenched or emitting labels as a function of their biological surroundings. Moreover, the fluorescence intensity of the labels can be significantly enhanced through the increase of their absorption cross section by involving a high number of fluorophores. This should decrease the detection threshold by enhancing the fluorescence contrast. This strategy has been recently followed by involving organic-dye-doped silica nanoparticles to detect DNA molecules [13]. About 10^4 fluorophores were dispersed inside a single nanoparticle of 100 nm in diameter which produced a strong fluorescence signal, greatly amplified compared to that of a single fluorophore. However, the synthesis of these silica nanoparticles is delicate because it implies several steps of surface functionalization to make hydrophobic organic dyes compatible with the hydrophilic surface of the nanoparticles. Furthermore, dispersed organic fluorophores in silica nanoparticles are submitted to a significant photobleaching, even if it is lower than that of the fluorescent molecules dissolved in solutions.

The aim of our work is to design a new type of fluorescent biochip whose signalization function (sensor transducer) is made up by ultra-bright fluorescent nanocrystals confined in silicate sol–gel thin films, with high sensitivity to biological surroundings. These molecular nanocrystals are composed of about 10^4–10^8 organic fluorophores as their size can be easily adjusted with the preparation conditions, from 20 to 800 nm in diameter. Such high numbers of molecules increase the corresponding absorption cross section of nanocrystals by several orders of magnitude, resulting in brilliant nano-objects which exhibit good photostabilities due to their crystallinity [14, 15]. Moreover, the crystal structure favors the delocalization of the fluorescence excitation through weak molecular coupling which leads, for selected organic nanocrystals, to their behavior as unique fluorescent transmitters [16]. These combined properties of the organic nanocrystals can lead to high fluorescence contrasts depending on the biological medium and thus to very low sensing thresholds.

The production of such organic nanocrystals is performed by a simple one-step generic process [17, 18]: the solution, containing the organic dye, sol–gel precursors, solvent, and a small amount of water, is aged for a few hours and then deposited by spin-coating on a substrate. The solvent evaporation at the end of the deposition leads to the polymerization of the silicate coating forming first a wet gel while the nucleation and growth of nanocrystals then take place in the pores of this gel. This confined nucleation avoids the nanocrystal coalescence and allows the control of their size. After drying, these nanocomposite thin films combine the good stability and easy handling of amorphous inorganic materials with the specific optical properties of organic nanocrystals. Our method can be applied to a large range of organic fluorophores: polyaromatic molecules, perylenes, stilbenes, bodipys etc. In this study, rubrene was selected as this fluorophore emits around 600 nm (orange-red), which is an appropriate wavelength to overcome biological noise by reducing the fluorescence background and lying in the biological transparency window. In addition, rubrene presents the advantage of exhibiting a simple signature; monoexponential fluorescence decay [19] with a fluorescence lifetime of 16 ns, which is longer than those of typical fluorophores used in biochips e.g. 1.5 ns for Cy5 and 3.6 ns for nile red [12].

On the other hand, our nanocrystallization method leads to buried nanocrystals in the sol–gel thin films that are thus well mechanically stabilized [18, 20]. The open porosity of the sol–gel coatings allows a selective reactivity between nanocrystals and their chemical surroundings. Indeed the pore size of silicate coatings can be easily modulated through the sol–gel chemistry to play the role of filter avoiding unwanted chemical interactions [21]. However, the pore size obtained by our sol–gel preparation cannot be higher than 10 nm. Indeed, in acidic conditions (pH $<$ 2), hydrolysis is faster than condensation. Thus, a low interconnected network is obtained which is limited to microporosity (1–2 nm) and weak mesoporosity (2–5 nm) [22, 23]. Furthermore, the rapid evaporation applied at the end of spin-coating is linked to very high capillary forces, leading to a maximal shrinkage, which ensures both the high quality of the films and the strong confinement of organic nanocrystals. This pore size is convenient for the development of chemical sensors, but is significantly smaller than the average size of biological molecules: several tenths of nanometers for DNA fragments. Therefore, to obtain nanocrystals potentially sensitive to their biological surroundings by direct contact, we have prepared emerging nanocrystals at the surface of the nanocomposite thin films. A first way would be to induce the organic nanocrystallization after impregnation of substrates, exhibiting large pores with diameters of around 50 nm [24, 25], by solutions. But this route requires a multi-step, delicate process, involving template agents, which is difficult to apply for the development of low cost fluorescent sensors.

In this work, the nanocrystals are first grown embedded in a sol–gel film as introduced above. Then, a specific and well-controlled chemical treatment is applied to partially dissolve the surface of the sol–gel layer to obtain nanocrystals emerging from silicate coatings, but remaining strongly anchored to the sol–gel thin films for good mechanical stability of the final sensing device. To obtain a controlled and reproducible dissolution process, the following parameters have been adjusted: the nature and concentration of the dissolving agent, dissolution rate, initial thickness of the films, and nanocrystal size. Nanocrystals emerging from the surface of dissolved films were then characterized by fluorescence confocal microscopy (FCM), atomic force microscopy (AFM), and time-resolved fluorescence spectroscopy.

2. Experimental details

2.1. Preparation of nanocrystals in sol–gel coatings

First, a solution was poured into an airtight flask containing THF (Aldrich, analytical grade), rubrene powder (Acros Organics, 99%), silicon alcoxides, and water. Two silicon alcoxides were used as sol–gel precursors: tetramethoxysilane (TMOS) from ABCR™ while 1,2-bis(trimethoxysilyl)ethane (TMSE) was synthesized [26]. The solutions were prepared from a TMOS:TMSE = 1:2 molar ratio. The hydrolysis–condensation reactions of these precursors were carried out under acidic catalyzed conditions (HCl, pH = 1) with one water molecule per alkoxide (–OCH_3) function ($h = [H_2O]/[–OCH_3] = 1$). The THF molar ratio referred to silicon alcoxides was $s = [THF]/[Si]$ with s between 10 and 20 ([Si] is the concentration of silicon alkoxide precursors) while the rubrene amount was $d = [rubrene]/[Si] = 1 \times 10^{-2}$, $s = 16$ for 800 nm-diameter nanocrystals, $d = 1 \times 10^{-3}$, $s = 16$ for 120 nm-diameter nanocrystals and $d = 1 \times 10^{-3}$, $s = 20$ for 60 nm-diameter nanocrystals. The solution was first heated at 80 °C for 4 h for the rapid rubrene dissolution and the enhancement of hydrolysis and condensation kinetics of the alcoxides, leading to the formation of silicate chains dispersed in solution. The resulting sols were then deposited at room temperature by spin-coating onto microscopic glass slides as substrates with a rotation speed of 4000 rpm applied for 5 s. Before deposition, to ensure a good adhesion, glass slides were first sonicated in a basic solution containing 5% in water of a basic commercial reagent (TFD4, Franklab SA) for 15 min, then washed several times in deionized water, and finally dried under nitrogen. When the sol was spread out on the substrate, the fast THF evaporation induced first the sol–gel polycondensation and a high dye supersaturation in the solution. This leads, at the end of the solvent evaporation, to the confined nucleation and growth of nanocrystals inside the pores of the silicate matrix. With this method, films with a thickness of around 0.3–0.5 μm were prepared. These nanocomposite coatings were then dried at 100 °C for 5 min.

2.2. Controlled dissolution of sol–gel thin films

The sol–gel coatings containing rubrene nanocrystals deposited onto microscope glass slides are plunged into stirred solutions containing etching or dissolving agents such as hydrofluoric acid HF and sodium hydroxide NaOH for various periods of time ranging between 1 and 16 h. In order to obtain homogeneous dissolutions, we chose a high volume of solution (800 ml) to avoid any significant evolution of the etching bath and also the redeposition of the dissolved silicate layer on the sol–gel thin films. Different HF and NaOH concentrations were tested ranging from 1 to 0.001 mol l^{-1}. Finally, sol–gel films were washed in a high volume of 18 MΩ water and dried under nitrogen.

2.3. Fluorescence confocal microscopy

The thinning of sol–gel coatings was first followed by fluorescence confocal microscopy (FCM) for a rapid and easy evaluation with a LSM510 Carl Zeiss microscope using a 63× oil-immersion objective (NA 1.4). The light excitation was produced by a (Ar or He–Ne) laser working at the wavelength $\lambda = 488$ nm. Fluorescence image data were then processed by Scion Image Software.

2.4. Atomic force microscopy

The surface dissolution of the sol–gel coatings was then accurately characterized by atomic force microscopy (AFM) performed in tapping mode with a nanoscope V microscope (Veeco). For all experiments, AC160TS silicon cantilevers with a force constant between 35 and 97 N m^{-1} were used. Tapping amplitudes were in the order of 150 mV. The excitation frequency was between 341 and 344 kHz. Height, amplitude, and phase images were recorded. AFM data were processed with the Nanoscope 7.2 software (Veeco).

2.5. Transmission electron microscopy

The transmission electron microscopy (TEM) images were obtained with a Philips CM300 under 300 kV. The samples were prepared by spinning the initial sol–gel solutions on NaCl cleaved crystal faces used as substrates. These substrates were then dissolved in large volumes of 18 MΩ water while the floating sol–gel films were placed on copper grids.

2.6. Time-resolved fluorescence spectroscopy

The measurements were performed with a titanium:sapphire laser pumped by an argon ion laser (82 MHz, repetition rate lowered to 4 MHz using a pulse-peaker) delivering very short impulsions of 1.3 ps. An optical nonlinear crystal of LBO was used to reach a 495 nm excitation through a second harmonic generation. Fluorescence signal detection was performed by a Europhoton GmbH photomultiplier. The samples were placed under a NIKON TE 2000 microscope and illuminated in a large field. Perfusion chambers (CoverWell™) of 35 μl were put on the samples to obtain fluorescence decays of the nanocrystals in the presence of different chemical environments. The functionalized DNA solution was provided by Eurogentec (reference: RPDDQ2B). The concentration of the solution was 100 μM l^{-1}.

3. Results and discussion

The sol–gel thin films containing rubrene nanocrystals were prepared using a well-established procedure [18]. They were deposited onto microscope glass slides by spin-coating and dried at 100 °C for a few minutes. Then, the films were dipped for different amounts of time into a large volume of stirred solution (1 l) of the dissolution agent. A typical dissolving method of silicate materials is to perform a chemical etching in HF acid solutions to transform Si–O bonds into Si–F (SiF_4 or H_2SiF_6) bonds that are highly soluble in aqueous solutions. HF aqueous solutions of different concentrations were tested for different etching times: from 30 s to 30 min. In all cases, the etching proved highly inhomogeneous with parts of the silicate films being completely removed, even

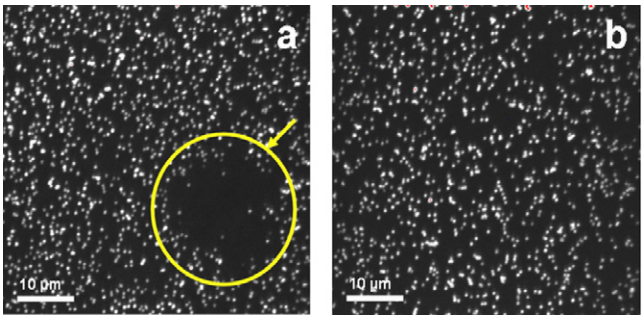

Figure 1. FCM images of sol–gel thin films containing rubrene nanocrystals (a) after a chemical etching in HF 10^{-1} M for 15 min and (b) after the controlled dissolution of the film surface with NaOH 10^{-1} M for 15 min.

at low HF concentrations (10^{-2}–10^{-3} M). This was directly observed by FCM, figure 1(a), where some sample areas are totally nanocrystal free. Indeed, the chemical etching happens preferentially at small defects of the films such as micro-holes due to a lack of wetting of the sol–gel solutions on the substrates at the first step of the spin-coating process. Thus, using HF as chemical agent, the process can be better described as an inhomogeneous chemical etching of the coating rather than a controlled dissolution of the film surface.

On the other hand, NaOH solutions are good solvents of silicate compounds while molecular crystals are generally insoluble in these aqueous media. Indeed, they are used for the crystal growth of α-quartz crystals under hydrothermal conditions [27] and, it has been shown that highly concentrated NaOH solutions allowed the thinning of quartz piezoelectric devices through a homogeneous dissolution of crystal plates [28]. Thus, NaOH aqueous solutions were then tested for the surface dissolution of sol–gel thin films. With a NaOH solution of 10^{-1} M, dissolution times of the film surface were evaluated around a few minutes before the loss of the nanocrystals from the silicate matrix. This corresponds to high dissolution rates of several tenths of nm min^{-1}. In contrast to HF solutions, we observed homogeneous dissolutions of the film surfaces without removing any silicate plates and fluorescent nanocrystals as shown by FCM (figure 1(b)). To achieve a better control of the surface dissolution of these nanocomposite coatings, lower kinetics are required. Thus, lower concentrations of NaOH were then tested, around 10^{-3} M, firstly on nanocomposite thin films involving large rubrene crystals of about 800 nm, as specified by FCM, with film thickness evaluated to 130 nm by a profilometry. Indeed, nanocrystals grow preferentially through the thickness of the layer confinement leading to stick-shaped crystals (figure 2). The dissolved surface of these coating was then characterized by AFM imaging in the tapping mode.

Figure 2(a) shows the AFM amplitude image of the film surface before dissolution exhibiting a significant roughness of about 40 nm root mean square (RMS), including the surface corrugation due to the underlying microcrystals. However, this value is weak compared to the crystal size because the crystal growth is confined in the depth of the coating. On the other hand, the roughness measured between organic crystals of around 0.5 nm RMS, corresponds to the typical low roughness generally obtained for sol–gel thin films processed by spin-coating. After 16 h of dissolution in NaOH 10^{-3} M, the sample aspect on the AFM image changes significantly at the crystal location: the surface dissolution of the silicate film reveals directly the surface of rubrene crystals with surface structure similar to the growth step while the surface of the sol–gel coating remains very smooth, around 0.5 nm RMS (figure 2(b)), as it was before the dissolution treatment. These first results confirm that we can prepare emerging organic nanocrystals at the surface of sol–gel thin films.

Smaller nanocrystals were then successfully grown in the sol–gel coatings by decreasing the initial rubrene concentration and adjusting the solvent amount in the starting sol–gel solutions [29]. An average diameter of 120 ± 20 nm was measured on TEM images (figure 3(a)). These nanocrystals exhibit a typical spherical shape as previously observed for different types of molecular crystals when their diameters are below 500 nm [30].

The sol–gel thin films were dissolved by a 10^{-3} M NaOH solution for 16 h. The resulting AFM image (figure 3(b)) clearly shows that all the nanocrystals emerge from the silicate surface after the film dissolution. The good control of the dissolution allows us to expose the nanocrystals while maintaining them in the thin films. Moreover, no degradation of the nanocrystal surface was observed by AFM after this dissolution of the matrix. For fluorescence decay measurements, to obtain single emitter behaviors associated to

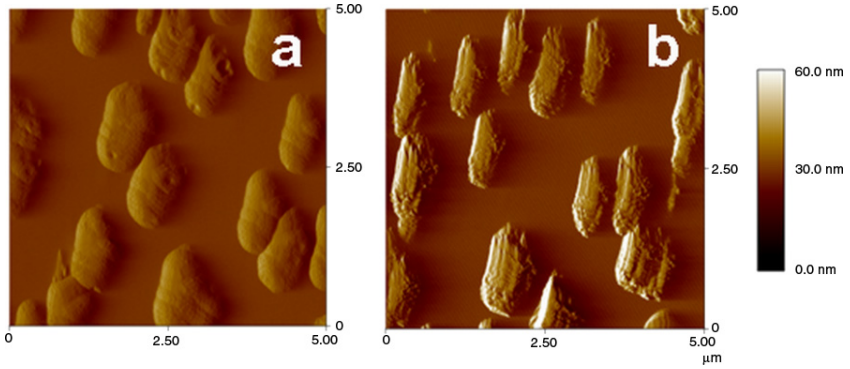

Figure 2. AFM amplitude images of 800 nm rubrene nanocrystals grown in sol–gel thin films (a) before chemical treatment and (b) after surface dissolution in NaOH 10^{-3} M for 16 h.

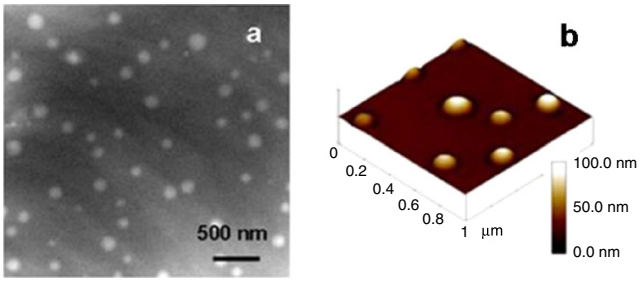

Figure 3. (a) TEM image of 120 ± 20 nm rubrene nanocrystals and the corresponding AFM 3D topography image of these nanocrystals, (b) after dissolution in NaOH 10^{-3} M for 16 h (3D topography).

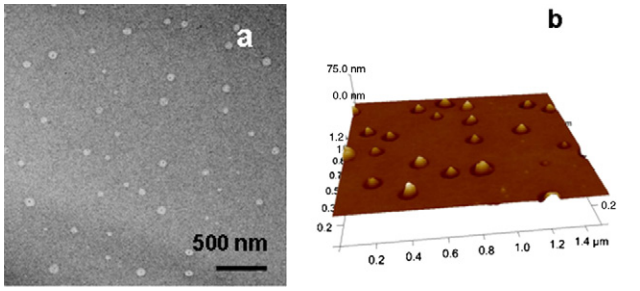

Figure 4. (a) TEM image of 60 ± 20 nm rubrene nanocrystals and corresponding AFM image of these nanocrystals, (b) after dissolution in NaOH 10^{-3} M for 8 h (3D topography).

strong fluorescence contrasts, we finally used smaller rubrene nanocrystals exhibiting diameters of 60 ± 20 nm characterized by TEM, figure 4(a). In this case, the sol–gel thin films were dissolved by a NaOH 10^{-3} M solution for 8 h leading to 60 nm nanocrystals emerging by about 10 nm from the silicate surface (AFM 3D topography images, figure 4(b)).

On the other hand, between nanocrystals, the very low roughness is conserved, thus confirming the high control of the homogeneous surface dissolution of the sol–gel thin films through a layer by layer mechanism. For NaOH 10^{-3} M solvent, the dissolution rate was measured around 2 nm h^{-1} for all the sol–gel coatings whatever the size of the embedded nanocrystals (figures 3 and 4). Indeed, the sol–gel thin films were prepared from the same alkoxides and experimental conditions leading to similar silicate structures. However, the dissolution time must be carefully defined. If the dissolution of the silicate matrix is too far advanced, the nanocrystals will be ejected from the sol–gel matrix.

The fluorescence decay of these emerging rubrene nanocrystals (60 ± 20 nm) was first recorded in the presence of water (figure 5(a)—red curve with triangles). The decay is almost monoexponential with a long fluorescence lifetime of 13.33 ns (92%) and a short fluorescence lifetime of 2.22 ns (8%). This fluorescence decay being similar to that of as-prepared nanocrystals embedded in the sol–gel layer (figure 5(a)—yellow solid curve) confirms that the fluorescence properties of hydrophobic rubrene nanocrystals are left intact by the NaOH treatment. Fluorescence decays of rubrene nanocrystals were then registered in the presence of a solution of DNA fragments (10^{-4} M) functionalized by dispersed blue 14 (DNA-DB14), which plays the role of the fluorescence quencher (molecular probe) in this case. Indeed, there is a strong overlapping between the fluorescence band of rubrene nanocrystals and the absorption band of DB14 in the visible wavelength region (figure 5(b)) that favors the Förster resonance energy transfer (FRET) [31]. In the presence of this DNA-DB14 solution, the fluorescence decay of the as-prepared buried nanocrystals (figure 5(a)—purple curve with circles) is barely modified in comparison to the initial one (yellow solid curve). This weak difference can be explained by some rubrene nanocrystals being located very close to the silicate surface, a few nanometers, thus being quenched by FRET with DNA-DB14 molecules adsorbed at the surface while the great majority of the buried nanocrystals which are well separated from the DB14 quencher remain fluorescent (scheme framed with purple). On the other hand, in the presence of the DB14-DNA solution, the fluorescence of emerging nanocrystals is strongly quenched (figure 5(a)—green curve with squares). The obtained decay is highly biexponential: the long fluorescence lifetime is unchanged (13.33 ns) but its ratio is lowered to 24%. This long fluorescence lifetime can be attributed to core molecules of the nanocrystals, which did not interact with the DB14-DNA solution. The short fluorescence lifetime (1.82 ns, 76%) corresponds to molecules of the nanocrystals whose fluorescence is quenched by the DB14-DNA solution. The DB14-DNA fragments inhibit by FRET the fluorescence of the great majority of rubrene nanocrystals that are located in their surroundings (scheme framed with green). This illustrates the strong dependence of the fluorescence properties of molecular nanocrystals on their biological surroundings and their single emitter behavior for diameters of several tenths of a nanometer.

These results represent a decisive step in the conception of new types of highly sensitive biochips: it demonstrates that DNA fragments functionalized with a quencher (molecular probe) can strongly inhibit the fluorescence of emerging nanocrystals (signalization function). The next step, in progress, is the grafting with covalent bonds of DNA fragments bearing a quencher (DNA-probe) on the nanocrystal surface. These functionalized quenched nanocrystals will allow the detection of DNA molecules (DNA-target) through their hybridization with the complementary DNA-probe grafted onto the nanocrystals. The DNA-target should be detected through the fluorescence recovering of nanocrystals. Such recovery could be based on a wavelength shift of the absorption band of the probe or on an increase of the nanocrystal—probe distance to stop the FRET quenching of nanocrystals. This recovery will induce significant intensity contrasts and lower detection thresholds, which are highly sought after features of biochip sensors.

4. Conclusion

In conclusion, to develop biological sensors with high sensitivity, we made directly available to biological aqueous solutions organic nanocrystals that were previously prepared embedded in sol–gel thin films. The selected route is the controlled dissolution of the sol–gel matrix surface covering the fluorescent nanocrystals by using weakly concentrated NaOH aqueous solutions. After this soft dissolution, the

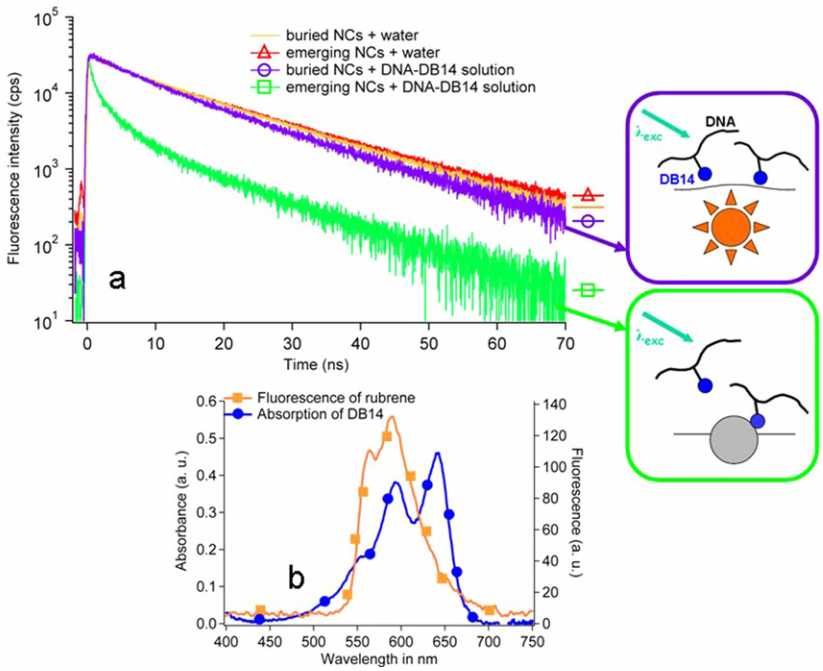

Figure 5. (a) Fluorescence decays of buried and emerging rubrene nanocrystals in the presence of water and in the presence of DNA-DB14 solution; corresponding schemes of buried and emerging nanocrystal behavior in the presence of DNA solution (insets). (b) Spectral overlapping between the fluorescence of rubrene and the absorption of DB14 favoring the FRET.

resulting silicate thin films present very low roughness, around 0.5 nm RMS. The nanocrystals emerging only by a few nanometers from the sol–gel surface are therefore mechanically stabilized. The molecular nanocrystals are fully insensitive to the NaOH aqueous solution as they keep their spherical shape and the same fluorescence properties. Hence, we have demonstrated the validity of this process of chemical dissolution of sol–gel films to obtain organic nanocrystals directly in contact with biological solutions. Therefore, they can be functionalized by grafting DNA-probe fragments to be integrated in biological sensor devices by playing the role of a generic signalization function (sensor transducer). This potential signalization function by emerging nanocrystals through the quenching of their fluorescence was demonstrated with solutions of DNA fragments functionalized with DB14. The realization of a biosensor now requires grafting these functionalizing DNA-probe fragments onto the nanocrystals, work which is already in progress. Finally, the perfectly controlled dissolution process developed in this study [32] through a layer by layer mechanism, involving weak concentrated NaOH solution, around 10^{-3} M, is a generic process that can be used for the thinning of any sol–gel layers, such as silicates, titanates, stanates, or zirconates. Low concentrations of other inorganic bases, LiOH or KOH for example, could also lead to well-controlled surface dissolution unlike the HF solutions that are usually used, which give rise to deep chemical etching in the sol–gel coatings.

Acknowledgments

This work was supported by the Research National Agency in France (ANR RIB) and the 'Délégation Générale pour l'Armement' (DGA).

References

[1] Cretich M, Damin F, Pirri G and Chiari M 2006 *Biomol. Eng.* **23** 77–88
[2] Park S H, Ko K C and Gwon H J 2007 *J. Labelled Compounds Radiopharm.* **50** 724–8
[3] Wiese R, Belosludtsev Y, Powdrill T, Thompson P and Hogan M 2001 *Clin. Chem.* **47** 1451–7
[4] Park S J, Taton T A and Mirkin C A 2002 *Science* **295** 1503–6
[5] Wang L, Lofton C, Popp M and Tan W 2007 *Bioconjug. Chem.* **18** 610–3
[6] Epstein J R, Biran I and Walt D R 2002 *Anal. Chim. Acta* **469** 3–36
[7] Sassolas A, Leca-Bouvier B D and Blum L J 2008 *Chem. Rev.* **108** 109–39
[8] Angenendt P 2005 *Drug Discov. Today* **10** 503–11
[9] Ekins R P 1998 *Clin. Chem.* **44** 2015–30
[10] Kusnezow W and Hoheisel J D 2003 *J. Mol. Recognit.* **16** 165–76
[11] Zhu H and Snyder M 2003 *Curr. Opin. Chem. Biol.* **7** 55–63
[12] Resch-Genger U, Grabolle M, Cavaliere-Jaricot S, Nitschke R and Nann T 2008 *Nat. Methods* **5** 763–75
[13] Zhao X, Tapec-Dytioco R and Tan W 2003 *J. Am. Chem. Soc.* **125** 11474–5
[14] Sanz N, Ibanez A, Morel Y and Baldeck P L 2001 *Appl. Phys. Lett.* **78** 2569–71
[15] Oikawa H, Masuhara A, Kasai H, Mitsui T, Sekiguchi T and Nakanishi H 2003 Organic and polymer nanocrystals: their optical properties and function *Nanophotonics: Integrating Photochemistry, Optics and Nano/Bio Materials Studies* ed H H Masuhara and S S Kawata (Amsterdam: Elsevier) (*Osaka, July 2003*)
[16] Botzung-Appert E, Monnier V, Duong T H, Pansu R and Ibanez A 2004 *Chem. Mater.* **16** 1609–11
[17] Ibanez A, Maximov S, Guiu A, Chaillout C and Baldeck P L 1998 *Adv. Mater.* **10** 1540–3
[18] Sanz N, Gaillot A C, Baldeck P L and Ibanez A 2000 *J. Mater. Chem.* **10** 2723–6

[19] Birks J B 1970 *Photophysics of Aromatic Molecules* (London: Wiley-Interscience)
[20] Botzung-Appert E, Zaccaro J, Gourgon C, Usson Y, Baldeck P L and Ibanez A 2005 *J. Cryst. Growth* **283** 444–9
[21] Monnier V 2006 Elaboration and structural characterisation of fluorescent molecular nanocrystals grown in sol–gel thin films for chemical and biological sensor applications *PhD Thesis* University Joseph Fourier, Grenoble
[22] Brinker C J, Hurd A J, Frye G C, Ward K J and Ashley C S 1990 *J. Non-Cryst. Solids* **121** 294–302
[23] Rouessac V, Van der Lee A, Bosc F, Durand J and Ayral A 2008 *Microporous Mesoporous Mater.* **111** 417–28
[24] Qi D, Kwong K, Rademacher K, Wolf M O and Young J F 2003 *Nano Lett.* **3** 1265–8
[25] Zhao Y, Yang D, Zhou C, Yang Q and Que D 2003 *J. Lumin.* **105** 57–60
[26] Boury B and Corriu R J P 2002 *Chem. Commun.* **8** 795–802
[27] Balitsky V S, Kurashige M, Balitskaya L V and Iwasaki H 2002 *J. Cryst. Growth* **237** 828–32
[28] Deleuze M, Goiffon A, Ibanez A and Philippot E 1995 *J. Solid State Chem.* **118** 254–60
[29] Monnier V, Sanz N, Botzung-Appert E, Bacia M and Ibanez A 2006 *J. Mater. Chem.* **16** 1401–9
[30] Oikawa H, Mitsui T, Onodera T, Kasai H, Nakanishi H and Sekiguchi T 2003 *Japan. J. Appl. Phys.* **42** L111–3
[31] Förster T 1959 *Discuss. Faraday Soc.* **27** 7–17
[32] Monnier V, Sanz N, Pansu R and Ibanez A 2008 Fluorescent organic nanocrystals for producing biosensors *Patent* WO/2008/145875